Metal ions doped TiO$_2$ nanotubes: synthesis, characterization and performance of metals doping in photocatalytic activity

R. C. Zulkifli[a], F. Azaman[b], M. H. Razali[a], A. Ali[b], M. A. A. M. Nor[a,*]
^{a} Faculty of Science and Marine Environment, Universiti Malaysia Terengganu 21030, Kuala Nerus, Terengganu, Malaysia
^{b} Faculty of Ocean Engineering Technology and Informatics, Universiti Malaysia Terengganu 21030, Kuala Nerus, Terengganu, Malaysia

Metal-ions doped TiO$_2$ nanotubes (M-TiO$_2$, M=Mn,Cr,Cu,Fe and Al) were synthesized using an in-situ hydrothermal method. The XRD pattern shown metal-ions doped TiO$_2$ nanotubes have an anatase phase. BET analysis shows that surface area was increased from 63.38 m^2/g to 138.44 m^2/g. The degradation rates of undoped-TiO$_2$, Mn-TiO$_2$, Cr-TiO$_2$, Cu-TiO$_2$, Fe-TiO$_2$, and Al-TiO$_2$ were 50%, 64%, 76%, 85%, 88%, and 93%, respectively. Al-TiO$_2$ showed the highest photocatalytic performance due to the smallest ionic radii, highest surface area, and smallest crystalline size. It can be seen that the degradation of 10 ppm of methylene blue solution was observed in the following order: Undoped-TiO$_2$<Mn-TiO$_2$<Cr-TiO$_2$<Cu-TiO$_2$<Fe-TiO$_2$<Al-TiO$_2$.

1. Introduction

Every year, an estimated 280 000 metric tonnes of textile dyes are discharged as industrial effluent around the world. It is expected that global demand for the textile industry is likely to increase by 2020 [1]. The release of dyes into the river or drain during textile fibre dyeing and finishing processes is a major source of water contamination [2]. The effects of continuous exposure to these wastes can threaten human health and marine life.

Alternatively, photocatalytic degradation using a metal oxide such as TiO$_2$ has been implemented to control and minimize wastewater pollution. TiO$_2$ is the most promising due to its ability to photodegrade organic dyes and properties such as non-toxicity, economic, high chemical and physical stability [3-6]. However, TiO$_2$ has some limitations due to its broad bandgap, 3.2 eV [7]. The rapid recombination of photogenerated electron-hole pairs may reduce photocatalytic performance. [8, 9]. Many studies, therefore, try to develop the efficiency of photocatalytic performance, such as by broadening the absorption range of TiO$_2$ in the visible region and reducing electron-hole recombination by using doping. A recent selection of TiO$_2$ doping cations and anions was introduced and investigated. TiO$_2$ doping with cations such as earth metal (Sc,Y and La), noble metals (Os, Pd, Ru, Rh, Ir, Ag and Pt), poor metals (Al, Ga, In, Pb and Bi), and transition metals (Fe, Co, Ni, Mn, Cr, V, Cu, Zn and Zr) have been reported [10, 11].

TiO$_2$ photocatalytic performance has been enhanced by doping with nonmetals (such as F, N, S, or B) or metals (such as Fe, Ag, Cu, Pd, Pt, or Ru) [12, 13]. Doping TiO$_2$ with noble metals such as Cu and Ag increases photocatalytic performance by changing its surface characteristics (e.g., surface area per mass, porosity) and widening the absorption range to the visible light.

Fe is one of the most suitable elements for industrial applications due to its low cost, easy preparation [15] and the Fe-doping induces the absorption edge's shift into the visible-light range with the bandgap's narrowing and lower the recombination of photogenerated holes and electrons [16]. Murashkina et al. [17] studied that the optimum Al ion concentration for Al dopant TiO$_2$ was 0.5 wt % (1 mmol) to get the highest photocatalytic activity. Others claimed that modified TiO$_2$

---

with Al ion inhibited TiO$_2$ transformation from anatase to rutile by maintaning the surface state of TiO$_2$ particles and limiting the growth of grain [18].

Various methods have been developed to synthesize TiO$_2$ nanostructures, such as template [19], sol-gel [20, 21], and hydrothermal [22]. Templates are resulting in spherical structural hollow particles of anatase TiO$_2$. The sol-gel method using starting materials such as titanium isopropoxide, titanium tetrabuthylorthotitanate, tetrabuthyltitanate, titanium ethoxide, or titanium tetrabutoxide has been used to synthesize nanoscales of TiO$_2$ but high temperatures are required [23]. The hydrothermal method has also been reported to synthesize TiO$_2$ nanoscales since the products developed by this method have a well-crystalline phase and a small crystalline size, supporting thermal stability and photocatalytic performance [24]. In this study, undoped TiO$_2$, Mn-TiO$_2$, Cr-TiO$_2$, Cu-TiO$_2$, Fe-TiO$_2$, and Al-TiO$_2$ were synthesized by an in-situ hydrothermal method due to easy preparation method and high capability to form large surface areas of nanostructured materials [25]. To the best of our knowledge, the lowest amount of each metal doped (1 mmol) that is incorporated into TiO$_2$ for the photocatalytic degradation of methylene blue has never been reported yet.

2. Materials and Methods

2.1. Materials

TiO$_2$ precursor powder, aluminium (III) nitrate nanohydrate, iron (III) nitrate nanohydrate, copper (II) nitrate trihydrate, chromium (III) nitrate nanohydrate, and manganese (II) acetate tetrahydrate were purchased from Merck. Solvents and other reagents were analytical grade and used without further purification.

2.2. Synthesis of Undoped TiO$_2$ and Metal-ions Doped TiO$_2$

TiO$_2$ powders were synthesized by an in-situ hydrothermal method as reported in a previous study report by Zulkifli et al. [26]. 2 g of titanium dioxide powder was mixed in a 100 mL of aqueous solution of 10 M NaOH and poured in a stainless-steel reactor lined with Teflon. The reactor was then transferred in an oven and heated at 150 °C for 24 hours. After completing the treatment, the remaining precipitate was filtered and washed with 1.0 M of HCl solution until pH 7 was reached. The obtaining percipitate was dried and placed in an oven at 80°C for 24 hours. After drying, the resulting powder was calcined at 500 °C. A similar procedure was followed to produce Mn-TiO$_2$, Cr-TiO$_2$, Cu-TiO$_2$, Fe-TiO$_2$, and Al-TiO$_2$, with an additional 1 mmol of each metal ion: manganese (II) acetate tetrahydrate, chromium (III) nitrate nanohydrate, copper (II) nitrate trihydrate, iron (III) nitrate nanohydrate, and aluminium (III). All the samples obtained were characterized using X-Ray Diffraction (XRD), Brunauer, Emmett, and Teller (BET), Scanning electron microscopy (*SEM*) micrographs, Field emission scanning electron microscopy (*FESEM*) micrographs and UV vis spectrometer. The X-Ray Diffraction (XRD) pattern was obtained with a Rigaku Miniflex with Cu-Kα (0.1541 nm) at scan rate from 10°- 80° (2θ). Crystallite size was calculated by using Scherrer's Equation using Eq. (1) stated below.

$$Scherrer's\ equation\ (D): \frac{k\lambda}{\beta \cos\theta} \tag{1}$$

where;

D = crystallite size in nm
K = 0.9 (constant)
λ = 0.1541 nm (wavelength of the X-ray radiation)
β = FWHM (full width at half maximum)
θ = the diffraction angle

The Surface area of the synthesized TiO$_2$ sample was determined using Brunauer, Emmett and Teller (BET) method based on the N$_2$ adsorption and desorption isotherms using a Quantachrome Nova 4200e automatic analyzer. SEM micrographs were captured using JSM 6360 Joey Scanning Electron Microscopy with an accelerated voltage of 15 kV and magnification of

10000X. FESEM micrographs were captured using the JSM-IT800 Joey with magnification at 100,000X.

2.3. Photocatalytic Performance test

Based on the previous report by Zulkifli et al. [26], the degradation test was performed by inserting 0.1 g of samples into 100 mL of 10 ppm methylene blue solution. The reaction mixture was agitated in the dark for 30 minutes before irradiation to reach absorption-desorption equilibrium between the catalyst and dye molecules. The suspension was then subjected to two hours of UV irradiation and continuously stirred. A UV bench lamp (302 nm, UV 230V, 50 Hz) provided the source of the UV light. Using a syringe, 5 mL of the aliquot was removed at every 30 minute of time interval and filtered via a 0.45 μm millipore filter. The absorption spectra were measured using a UV vis-spectrophotometer, and the percentage of methylene blue degradation was estimated using Eq.(2).

$$\% \ degradation = \frac{C_o - C_t}{C_o} \times 100 \tag{2}$$

where;

C_o is the initial absorption spectra of the dye

C_t is the absorption spectra of dye after reaction at t time

3. Results and Discussion

3.1. X-ray Diffraction

Fig. 1 shows the XRD patterns of undoped TiO_2, Al-TiO_2, Fe-TiO_2, Cu-TiO_2, Cr-TiO_2 and Mn-TiO_2. The anatase TiO_2 phase was assigned to all studied samples (101), (004), (200), (105), (211), (204), (116), and (215), as indicated by reflections at 2 = 25.26°, 37.78°, 48.00°, 53.93°, 54.00°, 62.78°, 70.19°, and 74.98°, respectively (JCPDS - 076, 173).

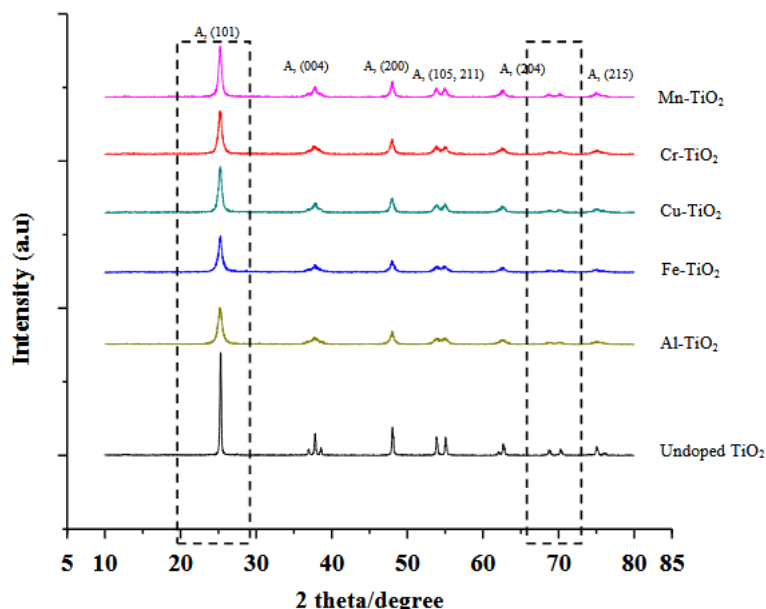*Fig. 1. XRD patterns of all samples after 2 hours of calcination at 500 °C*

Our results showed that doping does not alter the phase of the parent material, TiO_2. However, the anatase phase of undoped TiO_2, 25.26°, (101) has a narrow and sharp intensity, but the anatase peak and intensity of metal-ion doped TiO_2 were broadened and decreased

Furthermore, after doping, some peaks, such as 70.19° (116), shrank. These results indicated that the doping caused a distortion of the lattice structure of TiO_2 and affected the crystallinity of TiO_2 [28]. Based on the ionic radii of doping metal ions, Al^{3+} (0.53Å) and Fe^{3+} (0.69Å) are smaller and slightly the same compared to Ti^{4+} (0.64Å). It is favourable for these two metal ions to easily join the crystal structure, thus substituting the sites of Ti^{4+} [18]. Others, such as Cu^{2+} (0.72), Cr^{3+} (0.75), and Mn^{2+} (0.85), have larger ionic radii than Ti^{4+} and tend to reside in the TiO_2 lattice's interstitial position. Other workers have reported similar observations that have been interpreted as interstitial and substitute positions of the TiO_2 lattice site if metal ions have larger and smaller ionic radii than Ti^{4+} [29].

On the other hand, among the metal-ions doped TiO_2, Al-TiO_2 had the broader width peak, followed by Fe-TiO_2, Cu-TiO_2, Cr-TiO_2 and Mn-TiO_2 due to the small crystallite size. Generally, the crystallites exhibited smaller sizes due to the host lattice's growth being constrained by the dopant ions [30]. By applying Scherrer's equation, we have confirmed that the crystallite size of the Al-TiO_2 sample is smaller (11.14 nm) than the Fe-TiO_2 (11.50 nm), Cu-TiO_2 (12.32 nm), Cr-TiO_2 (15.98 nm), Mn-TiO_2 (15.30 nm) and undoped TiO_2 (38.38 nm) as listed in Table 1.

3.2. BET specific area

The surface area values, total pore volume, and pore size were obtained from the Brunauer, Emmett–Teller (BET) are listed in Table 1. The undoped TiO_2 has the lowest surface area, total pore volume, and pore size of about 63.38 m^2/g, 0.50 cm^3/g, and 32.13 nm, respectively. The Al-TiO_2 has the highest surface area, 138.44 m^2/g, a total pore volume of about 0.94 cm^3/g, and a pore size of 27.27 nm. For other doped-TiO_2 samples, the surface areas varied from 76.04 m^2/g to 136.26 m^2/g. It was observed that metal dopants affect the surface area of TiO_2 powder samples. The BET analysis results demonstrate that all samples have pore sizes ranging from 27.27 to 35.93 nm, classifying as mesoporous composites as per IUPAC notation. According to IUPAC notation, these materials are classified as mesoporous composites, with pore sizes ranging from 2 to 50 nm.

Table 1. Details characterization of undoped TiO_2 and metal ions doped-TiO_2 samples

Samples	Crystallite size (nm)	Surface area (m^2/g)	Total pore volume (cm^3/g)	Pore size (nm)
Undoped TiO_2	28.38	63.38	0.50	32.13
Al-TiO_2	11.14	138.44	0.94	27.27
Fe-TiO_2	11.50	136.26	0.96	28.10
Cu-TiO_2	12.32	103.51	0.81	31.55
Cr-TiO_2	15.98	82.02	0.65	31.95
Mn-TiO_2	15.30	76.04	0.76	35.93

3.3. Morphological characterization

The Electron Microscopy image shows almost identical morphology for all the doped samples (Fig. 2). Undoped TiO_2 morphology shows some agglomerated particles and bulk due to its larger crystal size. The undoped TiO_2 has a larger particle size than the doped TiO_2, consistent with the XRD study's crystal size calculation (Table 1). However, when a dopant metal ion is added, the agglomerated particles and bulk are less present and exhibit a smooth surface morphology. While all metal-ions doped TiO_2 has a homogeneous distribution in the SEM image, the morphology of Al-TiO_2 has changed with less agglomeration, and nanotube structures can be seen to crosslink irregularly on the surface (Fig. 3).
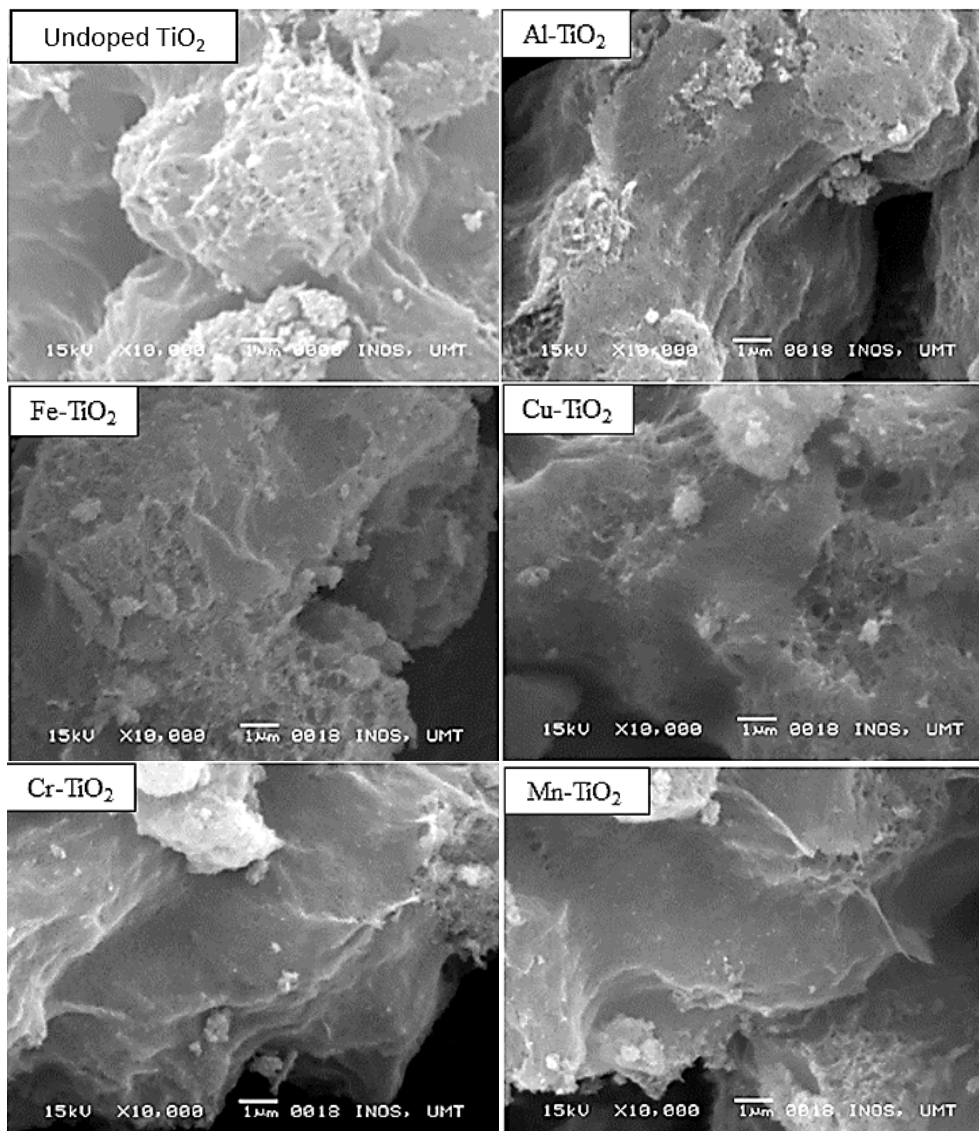
Fig. 2. SEM images of undoped TiO₂, Al-TiO₂, Fe-TiO₂, Cu-TiO₂, Cr-TiO₂, and Mn-TiO₂ after 2 hours calcination at 500 °C.
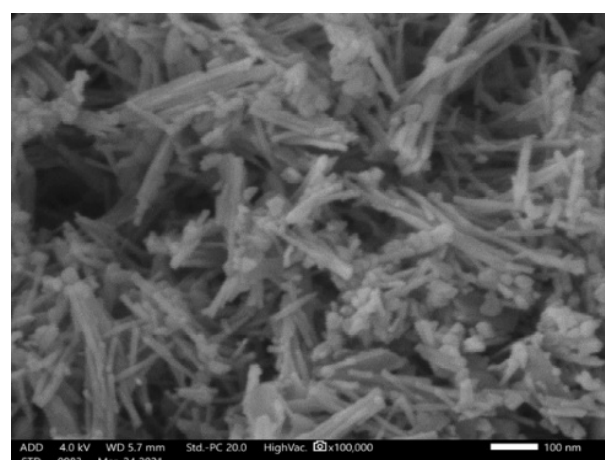
Fig. 3. FESEM images of Al-TiO₂ nanotubes after 2 hours calcination at 500 °C viewed under 100,000x magnification.

3.4. Optical Analysis

The optical absorption properties of mono doped TiO_2 were studied using UV–vis analysis. (Fig. 4 a). The photon energy of 3.24 eV in TiO_2 causes significant absorption at 400 nm, which can be attributed to the high absorption. Al, Fe, Cu, Cr, and Mn doping improved the optical absorption ability, resulting in a significant right shift in the absorption spectra towards longer wavelengths [31]. The absorption bands in the spectra for Al-TiO_2 were moved higher due to the reduced band gap in this case.
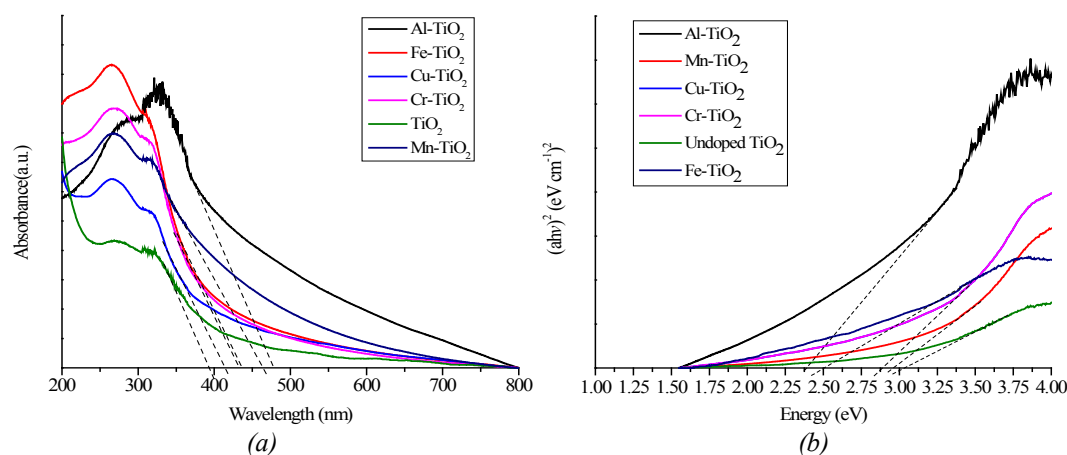

Fig. 4. UV-Visible spectra (a) and Tauc plots (b) of undoped TiO_2, Al-TiO_2, Fe-TiO_2, Cu-TiO_2, Cr-TiO_2, and Mn-TiO_2.

Doping of TiO_2 with Al, Fe, Cu, Cr, and Mn improved the optical absorption ability. The absorption bands in the spectra for Al-TiO_2 were moved higher due to the reduced band gap. As shown in Fig. 4 (b), the values of eg for Al-TiO_2, Fe-TiO_2, Cu-TiO_2, Cr-TiO_2, Mn-TiO_2, and undoped TiO_2 are 2.37 eV, 2.50 eV, 2.85 eV, 2.91 eV, and 3.0 eV, respectively.

Undoped TiO_2 shows a band gap of 3.0 eV, which is slightly lower than that reported by researchers. The band gap widens as the size of the particle shrinks due to electron confinement at the nanoscale. This phenomenon is known as the "quantum size effect"[32]. The charge transference band of O^{2-}-Ti^{4+}, which is modified by additional transference bands connected with doping cations, causes the red shift of the absorption and a reduction in band gap in all modified samples.

Doping with Al ions leads to the slowest shifting and shows a reduction of the band gap by 0.63 eV relative to undoped TiO_2. It can be concluded that the red shift of the absorption edge toward the visible light region was observed. The red shift demonstrated visible light absorption by revealing the presence of Ti-O-Al links and generating a new energy level in the bandgap of 2.37 eV, the lowest energy band gap recorded so far since Al-TiO_2 has typically been used in gas sensing [33]. This new finding contributed to the improvement of the Al doping TiO_2 towards photocatalytic studies.

3.5 Photocatalytic performance

A degradation test under UV light irradiation was used to evaluate the photocatalytic performance. The findings revealed that the photocatalytic performance increases as dopant is introduced. It is clearly seen that undoped TiO_2, has smallest photocatalytic performance (50%) while other with dopant such as Mn-TiO_2, Cr-TiO_2, Cu-TiO_2, Fe-TiO_2 and Al-TiO_2, are 64%, 76%, 85%, 88%, and 93%, respectively, as shown in Fig. 5. Besides, the highest photocatalytic performance was observed for the Al-TiO_2, which within 60 minutes was able to degrade 93% of 10 ppm of methylene blue solution due to its larger surface area. The highest photocatalytic performance of Al-TiO_2 could be due to its smallest ionic radii (0.53Å), its smallest crystalline size, and its largest surface area compared to Ti^{4+} (0.68Å) Thus, Al^{3+} was easily inserted into the lattice site structure of TiO_2 and altered the crystallite size of Al-TiO_2. Decreased crystalline size

can eventually lead to a larger surface area, which may increase the active site's surface area, resulting in increased absorption, electron-hole production, and interfacial carrier rate of degradation transfer [34].

Fe-TiO_2 also showed good photocatalytic degradation performance and yielded about 88 %. The light absorption of modified Fe-TiO_2 is extended due to an increase in the generation of electron-hole pairs, thus boosted light absorption in the visible spectrum. Fe^{3+} could serve as a h+/e trap to lower the rate of h+/e pair recombination and increase photocatalytic performance. Cu-TiO_2 was evaluated to give a good performance percent of 85% due to Cu doping, which reduces the band gap, red shifts the wavelength range for electron excitation, and increases light adsorption strength. The photocatalytic performance of Cr-TiO_2 showed that methylene blue degraded to 76%. This low photoactivity of Cr-TiO_2 is due to its small surface area and its ability to absorb hydroxyl groups that react with methylene blue.
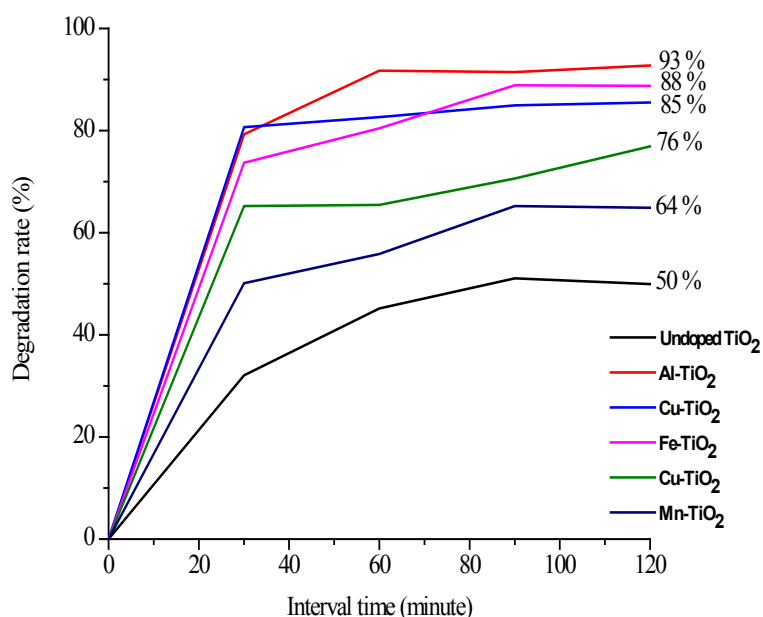

Fig. 5. Photocatalytic degradation of methylene blue at 10 ppm.

Mn^{2+} has the largest ionic radius (0.8Å) and may have a slightly have difficulty in entering the lattice and resulting in recombination. Another factor is the excess of trapped carriers in the Mn-TiO_2, causing the reducing of driving force to isolate the carriers. For smaller crystallites, usually, the recombination rate crystallites would outweigh the additional interfacial charge transfer process [35]. It can be seen that the removal of 10 ppm of methylene blue solution was observed in the following order: Undoped-TiO_2<Mn-TiO_2<Cr-TiO_2<Cu-TiO_2<Fe-TiO_2<Al-TiO_2.

Fig. 6 shows the schematic diagram of Al-TiO_2 photocatalysis for degradation of methylene blue. When electrons (e−) and holes (h+) move to the top layer of Al-TiO_2, the oxidation reaction occurs and the hole interacts with Al^{2+} to form Al^{3+}. Meanwhile, an electron at the covalent bond will undergo a reduction reaction, in which Al^{3+} formed Al^{2+}. The hydroxyl radical (•OH) and superoxide anion (•O_2) acts as an oxidant to degrade organic compounds. The organic compound will be converted into more ecologically friendly chemicals, like water and carbon dioxide, through a series of oxidation-reduction reactions.
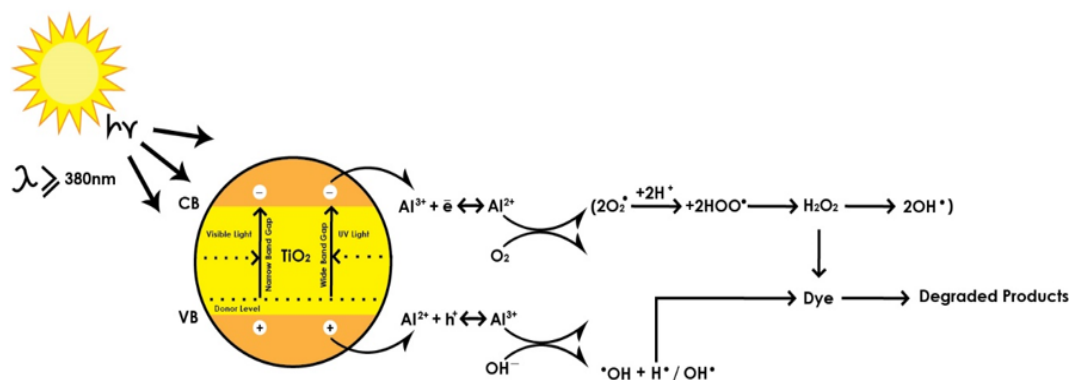
250

Fig. 6. Schematic diagram of Al-TiO$_2$ photocatalysis for degradation of methylene blue

5. Conclusions

In summary, undoped TiO$_2$, Mn-TiO$_2$, Cr-TiO$_2$, Cu-TiO$_2$, Fe-TiO$_2$, and Al-TiO$_2$ have been successfully synthesized using the in-situ hydrothermal method. All samples exhibited the anatase phase after being calcined at temperature 500°C with crystallite sizes in the range of 9.93-28.38 nm. The degradation of 10 ppm of methylene blue solution was observed in the following order: Undoped-TiO$_2$<Mn-TiO$_2$<Cr-TiO$_2$<Cu-TiO$_2$<Fe-TiO$_2$<Al-TiO$_2$. Based on these results, Al-TiO$_2$ showed the highest photocatalytic performance and has great potential to treat dye removal in the textile industry. The band gap energy for Al-TiO$_2$ was found to be the lowest band gap recorded so far. This new finding helped to improve the effect of Al doping TiO$_2$ in photocatalytic studies.

References

[1] Y.L. Pang, A.Z. Abdullah, Clean-Soil, Air, Water 41 (8), 751-764 (2013); https://doi.org/10.1002/clen.201000318
[2] A.E. Al Prol, Asian Fisheries Science, 3 (2),1-18 (2019); https://doi.org/10.9734/ajfar/2019/v3i230032
[3] M. Ijaz, M. Zafar, International Journal Of Energy Research 45 (3), 3569-3589 (2021); https://doi.org/10.1002/er.6079
[4] X. Kang, S. Liu, Z. Dai, Y. He, X. Song, Z. Tan, Catalysts 9 (2),191 (2019); https://doi.org/10.3390/catal9020191
[5] B. Pant, M. Park, S.J. Park, Coatings 9 (10), 613 (2019); https://doi.org/10.3390/coatings9100613
[6] W.J. Chen, K.C. Hsu, T.H. Fang, C.L. Lee, T.H. Chen, T. H. Hsieh, Digest Journal of Nanomaterial and Biostructures 16, 1227 (2021).
[7] M. Zhu, Y. Mi, G. Zhu, D. Li, Y. Wang, Y. Weng, Journal of Physical Chemistry C 117, 18863-18869 (2013); https://doi.org/10.1021/jp405968f
[8] H. Wang, L. Zhang, Z. Chen, J. Hu, S. Li, Z. Wang, J. Liu, X. Wang, Chemical Society Reviews 43 (15), 5234-5244 (2014); https://doi.org/10.1039/C4CS00126E
[9] W. Kim, T. Tachikawa, H. Kim, N. Lakshminarasimhan, P. Murugan, H. Park, T. Majima, W. Choi, Applied Catalysis A 147, 642-650 (2014); https://doi.org/10.1016/j.apcatb.2013.09.034

[10] A.S. Weber, A.M. Grady, R.T. Koodali, Catalysis Science & Technology 2, 683-693 (2012); https://doi.org/10.1039/c2cy00552b

[11] S.B. Patil, P.S. Basavarajappa, N. Ganganagappa, M.S. Jyothi, A.V. Raghu, K.R. Reddy, International Journal of Hydrogen Energy 44 (26), 13022-13039 (2019); https://doi.org/10.1016/j.ijhydene.2019.03.164

[12] T.M. Khedr, S.M. El-Sheikh, A. Hakki, A.A. Ismail, W.A. Badawy, D.W. Bahnemann, Photochemistry and Photobiology A: Chemistry 346, 530-540 (2017); https://doi.org/10.1016/j.jphotochem.2017.07.004

[13] M. Kudhier, R. Sabry, Y. Al-Haidarie, M. Al-Marjani, Materials Technology 33 (3), 220-226 (2018); https://doi.org/10.1080/10667857.2017.1396778

[14] P. Bezerra, R.P. Cavalcante, A. Garcia, H. Wender, M.A. Martines, G.A. Casagrande, J. Giménez, P. Marco, S.C. Oliveira, A. Machulek, Journal of the Brazilian Chemical Society 28, 1788-1802 (2017).

[15] J.Q. Li, D.F. Wang, Z.Y. Guo, Z.F. Zhu, Applied Surface Science 263, 382-388 (2012); https://doi.org/10.1016/j.apsusc.2012.09.066

[16] M. Wei, J. Wan, Z. Hu, Z. Peng, B. Wang, H. Wang, Applied Surface Science 391, 267-274 (2017); https://doi.org/10.1016/j.apsusc.2016.05.161

[17] A.A. Murashkina, A.V. Rudakova, V.K. Ryabchuk, K.V. Nikitin, R.V. Mikhailov, A.V. Emeline, D.W. Bahnemann, The Journal of Physical Chemistry C 122 (14), 7975-7981 (2018); https://doi.org/10.1021/acs.jpcc.7b12840

[18] S. Liu, G. Liu, Q. Feng, Journal of Porous Materials 17 (2), 197-206 (2010); https://doi.org/10.1007/s10934-009-9281-8

[19] X. Gao, B. Zhou, R. Yuan, Environmental Engineering Research 20 (4), 329-335. (2015); https://doi.org/10.4491/eer.2015.062

[20] S. Phromma, T. Wutikhun, P. Kasamechonchung, T. Eksangsri, C. Sapcharoenkun, Applied Sciences 10 (3), 993 (2020); https://doi.org/10.3390/app10030993

[21] R. Jothiramalingama, T. Radhika, P.R. Aswini, H. Al-Lohedan, M. Chandrasekaran, D.M. Al-Dhayan, J.N. Appaturi. Digest Journal of Nanomaterials & Biostructures 17(2), 491-497 (2022); https://doi.org/10.15251/DJNB.2022.172.491

[22] B. Niu, X. Wang, K. Wu, X. He, R. Zhang, Materials 11 (10), 1910 (2018); https://doi.org/10.3390/ma11101910

[23] N. Cotolan, M. Rak, M. Bele, A. Cör, L.M. Muresan, I. Milošev, Surface and Coatings Technology 307, 790-799 (2016); https://doi.org/10.1016/j.surfcoat.2016.09.082

[24] Y. Kondo, H. Yoshikawa, K. Awaga, M. Murayama, T. Mori, K. Sunada, S. Bandow, S. Iijima, Langmuir 24, 547-550 (2008); https://doi.org/10.1021/la702157r

[25] J. Zhu, F. Chen, J. Zhang, H. Chen, M. Anpo, Journal of Photochemistry and Photobiology A: Chemistry 180 (1-2), 196-204 (2006); https://doi.org/10.1016/j.jphotochem.2005.10.017

[26] R.C. Zulkifli, M.H. Razali, F. Azaman, A. Ali, M.A.A.M. Nor, Materials Science and Engineering 440 (1), 012019 (2018); https://doi.org/10.1088/1757-899X/440/1/012019

[27] X.Q. Cheng, C.Y. Ma, X.Y. Yi, F. Yuan, Y. Xie, J.M. Hu, B.C. Hu, Q.Y. Zhang, Thin Solid Films 615, 13-18 (2016); https://doi.org/10.1016/j.tsf.2016.06.049

[28] Y. Zhang, X. Xu, ACS Omega 5, (25), 15344-15352 (2020); https://doi.org/10.1021/acsomega.0c01438

[29] H. Feng, M.H. Zhang, E.Y. Liya, Applied Catalysis A: General 413, 238-244 (2012); https://doi.org/10.1016/j.apcata.2011.11.014

[30] M.H. Mamat, N. Parimon, A.S. Ismail, I.B.S. Banu, S.S. Basha, R.A. Rani, A.S. Zoolfakar, M.F. Malek, A.B. Suriani, M.K. Ahmad, Materials Research Bulletin 127, 110860 (2020); https://doi.org/10.1016/j.materresbull.2020.110860

[31] D. Li, H. Song, X. Meng, T. Shen, J. Sun, W. Han, X. Wang, Nanomaterials 10 (3), 546 (2020); https://doi.org/10.3390/nano10030546

[32] A.A. Issa, T.A. Hamoudi, Tikrit Journal of Pure Science 27 (3),15-18 (2022);

252

https://doi.org/10.25130/tjps.v27i3.55

[33] Y.J.Choi, Z.Seeley, A. Bandyopadhyay, S. Bose, and S.A. Akbar, 124 (1), 2007. Sensors and Actuators B: Chemical, 111-117 (2007); https://doi.org/10.1016/j.snb.2006.12.005

[34] S. Ghasemi, S. Rahimnejad, S.R. Setayesh, S. Rohani, M.R. Gholami, Journal of Hazardous Materials, 172 (2-3), 1573-1578 (2009); https://doi.org/10.1016/j.jhazmat.2009.08.029

[35] L.G. Devi, B.N. Murthy, S.G. Kumar, Materials Science and Engineering: B, 166 (1), 1-6. (2010); https://doi.org/10.1016/j.mseb.2009.09.008